JGR Atmospheres

RESEARCH ARTICLE
10.1029/2020JD033730

Special Section:
Fire in the Earth System

# Empirical Insights Into the Fate of Ammonia in Western U.S. Wildfire Smoke Plumes

**Jakob Lindaas[1], Ilana B. Pollack[1], Julieta Juncosa Calahorrano[1], Katelyn O'Dell[1], Lauren A. Garofalo[2], Matson A. Pothier[2], Delphine K. Farmer[2], Sonia M. Kreidenweis[1], Teresa Campos[3], Frank Flocke[3], Andrew J. Weinheimer[3], Denise D. Montzka[3], Geoffrey S. Tyndall[3], Eric C. Apel[3], Alan J. Hills[3], Rebecca S. Hornbrook[3], Brett B. Palm[4], Qiaoyun Peng[4], Joel A. Thornton[4], Wade Permar[5], Catherine Wielgasz[5], Lu Hu[5], Jeffrey R. Pierce[1], Jeffrey L. Collett Jr.[1], Amy P. Sullivan[1], and Emily V. Fischer[1]**

[1]Department of Atmospheric Science, Colorado State University, Fort Collins, CO, USA, [2]Department of Chemistry, Colorado State University, Fort Collins, CO, USA, [3]National Center for Atmospheric Research, Atmospheric Chemistry Observations & Modeling Laboratory, Boulder, CO, USA, [4]Department of Atmospheric Sciences, University of Washington, Seattle, WA, USA, [5]Department of Chemistry and Biochemistry, University of Montana, Missoula, MT, USA

**Abstract** Wildfires are a major source of gas-phase ammonia ($NH_3$) to the atmosphere. Quantifying the evolution and fate of this $NH_3$ is important to understanding the formation of secondary aerosol in smoke and its accompanying effects on radiative balance and nitrogen deposition. Here, we use data from the Western Wildfire Experiment for Cloud Chemistry, Aerosol Absorption, and Nitrogen (WE-CAN) to add new empirical constraints on the e-folding loss timescale of $NH_3$ and its relationship with particulate ammonium ($pNH_4$) within wildfire smoke plumes in the western U.S. during summer 2018. We show that the e-folding loss timescale of $NH_3$ with respect to particle-phase partitioning ranges from ~24 to ~4000 min (median of 55 min). Within these same plumes, oxidation of nitrogen oxides is observed concurrent with increases in the fraction of $pNH_4$ in each plume sampled, suggesting that formation of ammonium nitrate ($NH_4NO_3$) is likely. We find wide variability in how close our *in situ* measurements of $NH_4NO_3$ are to those expected in a dry thermodynamic equilibrium, and find that $NH_4NO_3$ is most likely to form in fresh, dense smoke plumes injected at higher altitudes and colder temperatures. In chemically older smoke we observe correlations between both the fraction of $pNH_4$ and the fraction of particulate nitrate ($pNO_3$) in the aerosol with temperature, providing additional evidence of the presence of $NH_4NO_3$ and the influence of injection height on gas-particle partitioning of $NH_3$.

**Key Points:**

- We estimate e-folding loss timescales for ammonia in eight western U.S. smoke plumes from 24 to 4000 min old (median = 55 min)
- Ammonium nitrate formation is favorable in fresh, dense plumes injected higher into the troposphere, nitric acid is normally limiting
- Observed ammonium and nitrate fractions increase with lower temperatures in medium (1–3 days) and old (>3 days) chemical aged smoke

**Supporting Information:**

Supporting Information may be found in the online version of this article.

**Correspondence to:**

J. Lindaas and E. V. Fischer,
jlindaas@rams.colostate.edu;
evf@rams.colostate.edu

**Citation:**

Lindaas, J., Pollack, I. B., Calahorrano, J. J., O'Dell, K., Garofalo, L. A., Pothier, M. A., et al. (2021). Empirical insights into the fate of ammonia in western U.S. wildfire smoke plumes. *Journal of Geophysical Research: Atmospheres*, *126*, e2020JD033730. https://doi.org/10.1029/2020JD033730

Received 19 AUG 2020
Accepted 20 MAY 2021

**Author Contributions:**

**Conceptualization:** Jakob Lindaas, Emily V. Fischer
**Data curation:** Jakob Lindaas, Ilana B. Pollack, Lauren A. Garofalo, Matson A. Pothier, Delphine K. Farmer, Sonia M. Kreidenweis, Teresa Campos, Frank Flocke, Andrew J. Weinheimer, Denise D. Montzka, Geoffrey S. Tyndall, Eric C. Apel, Alan J. Hills, Rebecca S. Hornbrook, Brett B. Palm, Qiaoyun Peng, Joel A. Thornton, Wade Permar, Catherine Wielgasz, Lu Hu, Amy P. Sullivan, Emily V. Fischer



## 1. Introduction

Wildfires are the largest natural terrestrial source of gas-phase ammonia ($NH_3$) to the atmosphere (Bouwman et al., 1997; Paulot et al., 2014) and these emissions may be growing in many regions of the world with increasing wildfire activity (e.g., Bray et al., 2018). $NH_3$ is the most abundant base in the atmosphere, and it can contribute to the formation of secondary inorganic (e.g., Behera & Sharma, 2010; Yokelson et al., 2009) and organic (e.g., Y. Liu et al., 2015) aerosol. This secondary aerosol has significant direct and indirect effects on the Earth's radiation budget, though the magnitude of these effects remains uncertain (Myhre et al., 2013; Paulot et al., 2017). $NH_3$ is a large fraction of the emitted reactive nitrogen ($N_r$) in wildfire smoke (Benedict et al., 2017; Lindaas et al., 2021; Roberts et al., 2020) and can also be an important source of reactive nitrogen to sensitive ecosystems via deposition as the smoke travels downwind (Chen et al., 2014; Karlsson et al., 2013; Prenni et al., 2014).

The magnitude of emissions of $NH_3$ from wildfires and the timescales of its fate in the atmosphere are both uncertain. Accurate and precise *in situ* measurements of gas-phase $NH_3$ are difficult due to its polarity and affinity for adsorption to surfaces (Pollack et al., 2019). Satellite retrievals of total column $NH_3$ hold promise for estimating emissions of $NH_3$ (Dammers et al., 2019), but efforts to infer the magnitude of $NH_3$ emission factors using satellite data from fires often rely on a prescribed value for the effective lifetime of $NH_3$ in smoke (Whitburn et al., 2015).

**Formal analysis:** Jakob Lindaas
**Funding acquisition:** Delphine K. Farmer, Sonia M. Kreidenweis, Joel A. Thornton, Lu Hu, Emily V. Fischer
**Methodology:** Jakob Lindaas, Julieta Juncosa Calahorrano, Katelyn O'Dell, Jeffrey R. Pierce, Jeffrey L. Collett, Amy P. Sullivan, Emily V. Fischer
**Project Administration:** Delphine K. Farmer, Joel A. Thornton, Emily V. Fischer
**Software:** Jakob Lindaas
**Supervision:** Emily V. Fischer
**Visualization:** Jakob Lindaas
**Writing – original draft:** Jakob Lindaas
**Writing – review & editing:** Jakob Lindaas, Ilana B. Pollack, Julieta Juncosa Calahorrano, Katelyn O'Dell, Lauren A. Garofalo, Delphine K. Farmer, Rebecca S. Hornbrook, Brett B. Palm, Qiaoyun Peng, Joel A. Thornton, Lu Hu, Jeffrey R. Pierce, Jeffrey L. Collett, Amy P. Sullivan, Emily V. Fischer

Few studies have empirically quantified the loss timescale of gas-phase $NH_3$ in biomass burning smoke plumes. Those that do most often call the estimated loss timescale a "lifetime" or "effective lifetime." However, the loss of gas-phase $NH_3$ is likely more complicated than a first-order exponential decay toward zero. Oxidation is very slow, deposition to the ground is usually negligible, and it is generally assumed that gas-phase $NH_3$ in smoke is lost by partitioning to the particle-phase via equilibrium-driven processes. These processes are dependent on $T$ and RH and complicated by ongoing plume dilution and changing acid concentrations. Thus, while we report the estimated literature values in the same terms used by each analysis, we will employ the term "e-folding loss timescale toward quasi-equilibrium" or "e-folding loss timescale" in our own analysis (Section 2.3.4).

*In situ* observations from aerosol mass spectrometers and Particle-into-Liquid samplers have inferred that ammonium nitrate ($NH_4NO_3$) is quickly formed (within minutes to hours) in smoke plumes based on the presence of both ammonium ($NH_4^+$) and nitrate ($NO_3^-$) species or ions (Akagi et al., 2012; Alvarado et al., 2010; Hobbs et al., 2003; Kleinman et al., 2008; X. Liu et al., 2016; Yokelson et al., 2009). Abundant $NH_3$ in smoke accompanied by the oxidation of co-emitted nitrogen oxides ($NO_x$) is commonly assumed to lead to rapid association of $NH_3$ with nitric acid ($HNO_3$). However, several studies have acknowledged or offered evidence for the association of $NH_3$ with organic acids to form organic ammonium salts (Akagi et al., 2012; Song et al., 2005). Other studies have reported enhancements of particulate ammonium and/or nitrate ($pNH_4$; $pNO_3$) in smoke but did not attribute these enhancements to specific causes or compounds (Benedict et al., 2017; Collier et al., 2016; Hecobian et al., 2011).

Given the present uncertainties in $NH_3$ evolution and the processes driving $NH_3$ aging in smoke, there is a need for additional empirical constraints on the e-folding loss timescale of $NH_3$ and its relationship with $pNH_4$ within wildfire smoke plumes (Paulot et al., 2017). Here, we use data from the 2018 Western Wildfire Experiment for Cloud Chemistry, Aerosol Absorption, and Nitrogen (WE-CAN) field campaign to derive empirical insights into $NH_3$ evolution in wildfire smoke. These data dramatically expand the limited number of fires for which $NH_3$ aging has been characterized. First, we estimate the e-folding loss timescales and distances of gas-phase $NH_3$ decreases with respect to gas-particle partitioning, as well as the e-folding loss timescales and distances with respect to dilution and partitioning. These loss timescales can be compared with the e-folding production timescale estimated from observed increases in $pNH_4$. Next, we explore the connection between $NO_x$ oxidation chemistry and $NH_3$ aging, and investigate the conditions under which thermodynamic equilibrium may favor $NH_4NO_3$ formation. Lastly, we calculate the fraction of $pNH_4$ and $pNO_3$ in older smoke and find anti-correlations with temperature, suggesting the smoke plume injection heights and transport pathways influence gas-particle partitioning of $NH_3$ through the abundance and equilibrium of $NH_4NO_3$.

## 2. Methods

### 2.1. Pseudo-Lagrangian Sampling Strategy

The WE-CAN field project used the instrumented National Science Foundation/National Center for Atmospheric Research (NSF/NCAR) C-130 research aircraft to sample smoke from wildfires across the western U.S. between July 22, and September 13, 2018 (https://www.eol.ucar.edu/field_projects/we-can). The C-130 aircraft payload was organized to specifically probe the evolution of reactive nitrogen ($N_r$) in wildfire plumes, along with absorption properties of smoke aerosol, cloud-smoke interactions, and near-source smoke chemistry. Approximately two thirds of the 134 total flight hours were allocated to sampling emissions and aging of daytime plumes. Wildfire smoke plumes were typically sampled during their first day of atmospheric evolution and pseudo-Lagrangian sampling was attempted for 12 fires. Flight patterns typically involved sampling background conditions immediately upwind of the fire followed by sampling the downwind smoke plume in a "lawn-mower" pattern as shown in Figure 1. The plume was transected perpendicular to its direction of downwind travel, with the first transect being performed as close to the fire as possible, ranging between 18 and 54 min (mean = 38 min) estimated physical age for the fires included in this analysis (Section 2.3.3). Using real-time wind speed and direction measurements aboard the aircraft, downwind transects could be planned with the intention of repeatedly intercepting the same parcel of smoke as it was advected downwind. This sampling pattern was generally performed at a constant altitude, which was determined from the injection height of the thickest portion of the smoke plume. Changes in

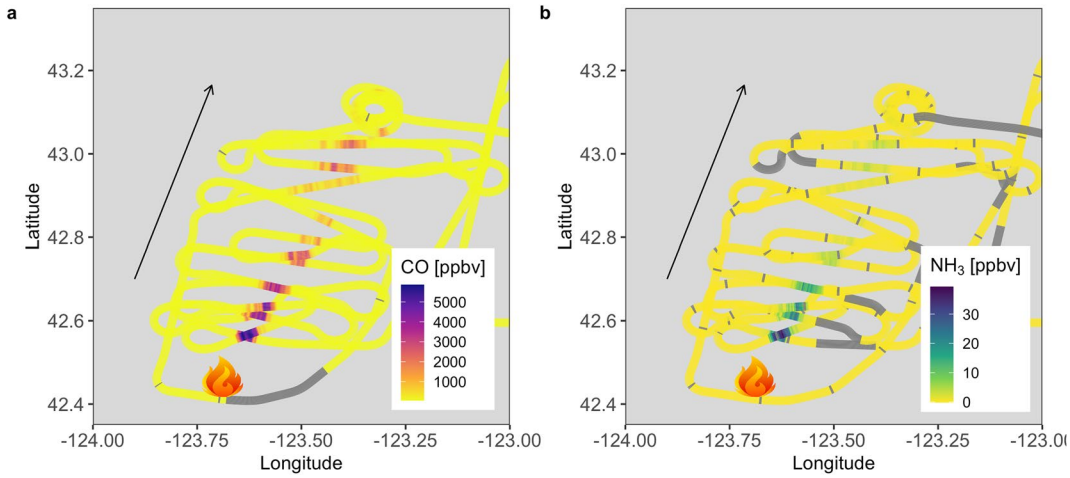


**Figure 1.** National Center for Atmospheric Research/National Science Foundation C-130 flight track around the Taylor Creek Fire, July 30, 2018 during Research Flight 3 (RF03), colored by (a) CO and (b) $NH_3$ mixing ratios. The black arrow shows the average wind direction and the fire icon shows the fire location. Gray periods in the flight track indicate calibration and/or instrument zero periods or other periodical instrument checks.

altitude were occasionally necessary to better follow the center portion of the smoke plume or were part of the flight plan to sample different parts of the plume's vertical structure. In some cases, unplanned altitude changes were necessitated by air traffic control. More details about the WE-CAN field project and other sampling strategies may be found in Lindaas et al. (2021).

### 2.2. Measurements

The WE-CAN payload included a large suite of gas- and particle-phase measurements relevant to the fate of $NH_3$ species. Instruments used to measure the species used in this analysis include: the National Center for Atmospheric Research (NCAR) 2-channel and single-channel chemiluminescence instruments for the measurement of nitrogen oxide, nitrogen dioxide, and ozone (NO, $NO_2$, and $O_3$); the Colorado State University quantum cascade tunable infrared laser direct absorption spectrometer (CSU QC-TILDAS) for the measurement of gas-phase $NH_3$; the University of Washington iodide-chemical ionization mass spectrometer (UW I-CIMS) for the measurement of hydrogen cyanide, nitric acid, nitrous acid, and multifunctional organic nitrates (HCN, $HNO_3$, HONO, ONs); the NCAR PAN-CIMS for the measurement of peroxyacetyl nitrate (PAN) and peroxypropionyl nitrate (PPN); the University of Montana proton transfer reaction time-of-flight mass spectrometer (UM PTR-ToF-MS) for the measurement of acetonitrile ($CH_3CN$); the CSU aerosol mass spectrometer (AMS) for the measurement of particulate-phase ammonium and nitrate ($pNH_4$ and $pNO_3$); the NCAR QC-TILDAS for the measurement of carbon monoxide (CO) and nitrous oxide ($N_2O$); the NCAR Picarro for the measurement of carbon dioxide, carbon monoxide and methane ($CO_2$, CO, and $CH_4$); and the NCAR Trace Organic Gas Analyzer (TOGA) for the measurement of 2-methylfuran, acrolein, and acrylonitrile. Full instrument descriptions and related references are reproduced in the SI with permission from Lindaas et al. (2021) and O'Dell et al. (2020) (for TOGA).

### 2.3. Calculation Methods and Data Treatments

#### 2.3.1. Plume Transect Criteria

A plume transect is defined as an individual flight segment that perpendicularly transects a smoke plume with background air present on both sides. Start and end times for plume transects were visually identified when the time series of CO, HCN, and $NH_3$ all concurrently and sharply deviated from their average background mixing ratios. For reproducibility, we have included a file with the start and stop times for each plume transect in the SI. If one or more of these measurements was missing (e.g., during a calibration) additional tracers were employed such as PAN and $NO_2$. CO and HCN are considered to be conservative

tracers on the timescales of interest here (0–5 h of physical transport) given their lifetimes of ~10 days and ~3 months, respectively, during summer (Holloway et al., 2000; Li et al., 2000). Plume transects attributed to a single fire are grouped for further analysis.

#### 2.3.2. Normalized Excess Mixing Ratio (NEMR)

The NEMR enables comparison of abundances between and within plumes (Yokelson et al., 2013). By accounting for dilution through normalizing a given measurement by a conserved tracer such as CO, we can investigate changes in abundances due to chemical production or consumption, as well as differences in emissions and aging between plumes. Here, we calculate the NEMR of species $X$ for a given plume transect by calculating the integrated $\Delta X$ ($= \Sigma[X_{measured} - X_{background}]$) and the integrated $\Delta CO$ ($= \Sigma[CO_{measured} - CO_{background}]$) and dividing $\Delta X$ by $\Delta CO$. Backgrounds for CO and the species $X$ are calculated as the mean of 15 s of measurements before and after a given plume transect's start and end times, respectively. Data points with missing measurements of either $X$ or CO are not included in this calculation, and most observations included in this analysis were reported at 1-Hz or faster. AMS data were reported on a 5-s timebase in standard mass concentration units, and these data are converted to an ambient mixing ratio equivalent before merging them with the other 1-Hz data for analysis. Reported precision and accuracy as well as the standard deviation in the background estimates for $X$ and CO are summed in quadrature to calculate an uncertainty for the NEMR of a given species over each plume transect.

#### 2.3.3. Physical and Chemical Age Estimates

We estimate the physical age of a plume by dividing the distance between the fire emission source and each downwind plume transect by the plume wind speed. The distance is measured from the centroid of the active burn area on that day to the center of the plume transect, and wind speed is estimated as the average wind speed across all downwind plume transects sampled for that fire. If a smoke plume from a given fire was followed downwind and the sampling pattern was repeated, a separate average wind speed was calculated from the second set of passes and used to estimate the physical age of the transects in that pseudo-Lagrangian pattern. Estimated physical ages could deviate from the true plume age at each transect due to several factors including variable wind speeds along the aircraft and plume trajectories, uncertainties in the active burn location, and differences in atmospheric friction and entrainment. We estimate the uncertainty in our calculations of physical age using the 1-sigma standard deviation in the mean wind speed across each set of plume transects. Uncertainty in the fire location at the specific time of sampling is not available. To assess the efficacy of attempted pseudo-Lagrangian sampling efforts, an estimated emission time ($t_0$) was calculated for each plume transect by subtracting the estimated physical age from the time the plume transect occurred. Most sets of plume transects contained transects all with estimated $t_0$ within 2 h. Fires with Pseudo-Lagrangian sampling patterns with sets of transects containing $t_0$ differences >2 h were excluded from this analysis in order to limit the possible influence of time-varying emissions and evolution on our analysis. We also excluded plume intercepts that were not connected to the intended pseudo-Lagrangian sampling efforts (i.e., sampled smoke from other fires nearby or from portions of the plume not entrained in the mean atmospheric flow). See the SI for a full list of plume transect start and stop times. Since the lifetime of both HCN and CO are much greater than the elapsed sampling time, we would expect HCN NEMRs to remain constant with plume physical age in a true Lagrangian sampling system. In the eight pseudo-Lagrangian sampling cases identified, HCN NEMRs were confirmed to remain within initial propagated error during the time spent sampling the plume (Figure S1).

We also assigned a broader set of smoke plume intercepts an approximate chemical age following O'Dell et al. (2020). This assignment of chemical age is useful because it allows us to examine the partitioning of $NH_x$ in all the smoke samples intercepted during WE-CAN, not just those that were sampled in a pseudo-lagrangian fashion from known fires. Briefly, smoke-influenced data were identified using co-elevated CO > 85 ppbv, HCN > 275 pptv, and $CH_3CN$ > 200 pptv. Smoke-influenced data were assigned an approximate chemical age using three VOCs with different second-order reaction rate constants for loss via reaction with OH: 2-methylfuran ($k_{OH} = 7.31 \times 10^{-11}$ cm$^3$ molecule$^{-1}$ s$^{-1}$, Aschmann et al., 2011), acrolein ($k_{OH} = 1.96 \times 10^{-11}$ cm$^3$ molecule$^{-1}$ s$^{-1}$, Atkinson, 1986; NIST Chemical Kinetics Database), and acrylonitrile ($k_{OH} = 4.04 \times 10^{-12}$ cm$^3$ molecule$^{-1}$ s$^{-1}$, Harris et al., 1981; NIST Chemical Kinetics Database). Based on which of these three VOCs is above background abundances in a plume, O'Dell et al. (2020) grouped smoke samples into three bins. Young smoke has an estimated age of <1 day, the medium smoke group includes

smoke plumes with estimated ages of 1–3 days, and all smoke with estimated chemical ages >3 days is categorized as old smoke. While this method likely captures the general progression of chemical aging in smoke, there are limitations: the binning of smoke samples is impacted by the age tracer dilution as well as chemistry, and the age assignments do depend on an assumed constant smoke OH concentration.

#### 2.3.4. Exponential Fitting of Empirical Relationships

We calculate first-order exponential decay toward a quasi-equilibrium value (Equation 1) and asymptotic growth (inverse exponential decay; Equation 2) equations to fit the change in calculated $NH_3$ and $pNH_4$ NEMRs respectively with estimated plume age (nls and SSasymp functions: *R* software, package "stats," v3.5.1). These equations are fit separately to the NEMRs for each species and set of plume transects. The estimated timescale with respect to loss or production is the inverse of the exponential coefficient, $\tau = \frac{1}{k}$. Here, we call $\tau$ the e-folding loss (production) timescale. A first-order exponential decay to zero equation (Equation 3) is also fit to the enhancement mixing ratios above background of $NH_3$ and CO for each set of plume transects. The inverse of the exponential coefficient, $\tau = \frac{1}{k}$, of these fits is an estimate of the e-folding timescales (or distances if fit using the distance from the fire) with respect to dilution plus chemistry ($NH_3$), and just dilution (CO).

$$y = y_{asymptote} + (y_0 + y_{asymptote}) * e^{-kx} \quad (1)$$

$$y = y_{asymptote} * (1 - e^{-kx}) \quad (2)$$

$$y = y_0 * e^{-kx} \quad (3)$$

Because we did not sample the plumes exactly at the emission source ($t_0$), we make one important assumption about the $NH_3$ and $pNH_4$ NEMR fits. All $NH_3$ and $pNH_4$ is assumed to be in the form of gas-phase $NH_3$ at emission. Accordingly, a calculated $NH_3$ NEMR data point of magnitude $NH_3$ NEMR + $pNH_4$ NEMR from the closest transect to the fire is added at $t_0$ and used in calculating the e-folding loss timescale of $NH_3$ NEMR for each plume. Likewise a $pNH_4$ NEMR point of magnitude zero is added at $t_0$ and used in the calculation of the $pNH_4$ NEMR e-folding growth timescale. With this assumption, we are able to estimate the rate of rapid partitioning often occurring in the minutes before the aircraft was able to sample the plume. We did test the sensitivity of the estimated loss and growth timescales to this initial assumption and found no change outside error for relaxed assumptions of down to 50% of $pNH_4$ assumed to be $NH_3$ at emission.

## 3. Results and Discussion

Figure 1 shows the sampling pattern downwind of the Taylor Creek Fire sampled on July 30, 2018 during RF03. The flight track is colored by CO (1a) and $NH_3$ (1b) mixing ratios with darker colors indicating the plume core as the aircraft transited the smoke plume. Transects further downwind contained progressively less CO (evidence of dilution) and $NH_3$ (evidence of dilution plus chemistry). The Taylor Creek Fire plume was a discrete plume that was injected above the boundary layer and entrained into the free-tropospheric flow. The aircraft was nearby when the plume pushed up and out of a smoke-filled boundary layer, and this time was noted. As the plume dispersed, the front edge of the plume continued to be visible because the surrounding free tropospheric air was quite pristine. However, the plume was also sufficiently large enough to also be easily intercepted by the aircraft. This fire afforded the best opportunity to repeatedly sample a a very fresh plume using a pseudo-Lagrangian flight pattern. The estimated emission times ($t_0$, described in section 2.3.3) for most of the individual plume transects shown in Figure 1 are within 1 h (during a several-hour flight time), indicating the pseudo-Lagrangian sampling was effective. We have identified seven other cases of pseudo-Lagrangian sampling where the estimated emission times from individual passes were within ~2 h of each other. The Bear Trap Fire (August 9, 2018; RF09) plume was sampled with two separate pseudo-lagrangian patterns and the South Sugarloaf Fire (August 26, 2018; RF15) plume was sampled at multiple altitudes at each distance downwind. These cases were separated and kept distinct during this analysis. Thus, the eight pseudo-Lagrangian sampling cases correspond to six individual fires.

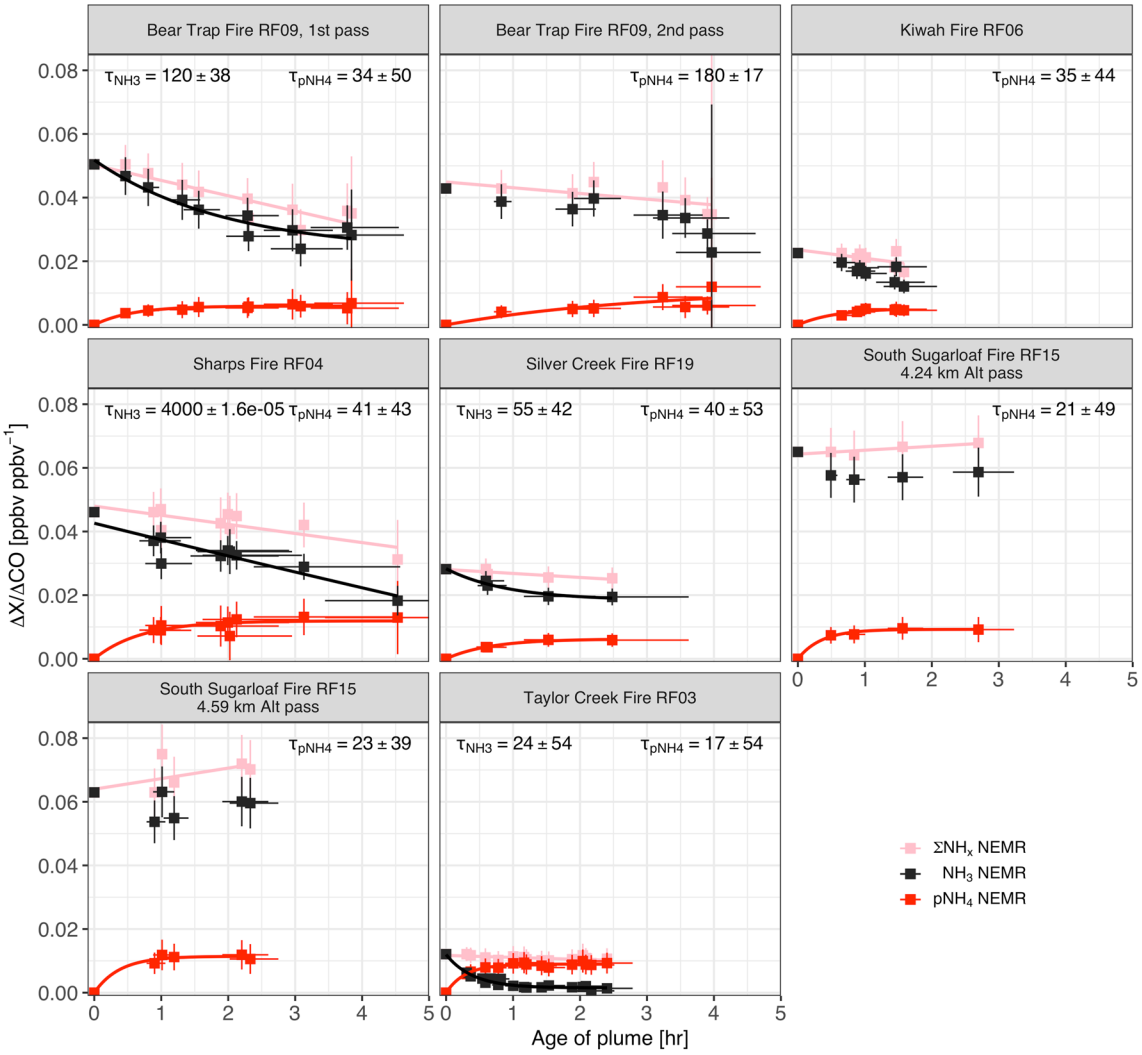


**Figure 2.** Evolution of ammonia ($NH_3$) and particulate ammonia ($pNH_4$) normalized excess missing ratios (NEMRs) with estimated physical plume age. The sum of $NH_3$ and $pNH_4$ is shown in pink points, $NH_3$ is in black, and $pNH_4$ is shown in red, with empirical fits plotted as lines. Points at time 0 are assumed NEMRs. Empirical fits are an exponential decay to a quasi-equilibrium value for $NH_3$, and an asymptotic increase (inverse exponential decay) for $pNH_4$. $\tau_{NH3}$ and $\tau_{pNH4}$ represent the estimated e-folding time with respect to chemical losses and chemical production respectively, ±1-sigma standard deviation in minutes. No estimate for the e-folding time is shown if the fit did not converge.

Measurements of gas-phase $NH_3$ and aerosol species such as $pNH_4$ from the AMS are tightly correlated with CO in fresh and old smoke in the WE-CAN data set ($R^2 = 0.68$ for $NH_3$ and CO over all plume transects); and $NH_3$ enhancements above background reached >400 ppbv in fresh smoke. Distinct enhancements of $NH_3$ of >1 ppbv are generally present even in old smoke (Figure S2a), while detectable background mixing ratios of ~0.2–1 ppbv are present in the clean free troposphere. Figure 2 shows the evolution of dilution-corrected gas-phase $NH_3$, $pNH_4$, and the sum of $NH_3$ and $pNH_4$, $\Sigma NH_x$. While six out of the eight plumes are observed to lose $NH_3$ with physical aging, both altitudes of the South Sugarloaf plume maintain roughly constant $NH_3$ NEMRs and $pNH_4$ NEMRs appear to increase. If all the $NH_3$ lost from the gas-phase partitions to the aerosol, in a perfectly Lagrangian-sampled plume we would expect $\Sigma NH_x$ to remain constant after correcting for dilution. We observe steady or slightly decreasing $\Sigma NH_x$ NEMRs with estimated physical age for all fires with the exception of South Sugarloaf. Several of the apparent decreases are within the propagated uncertainty of the measurements and NEMR calculations. Background errors become larger as the plume dilutes and enhancements above background are less pronounced. However, the decrease in the Bear Trap smoke plume is outside the propagated uncertainty, and represents ~40% loss of $\Sigma NH_x$ over ~4 h of physical aging. A possible explanation for "missing" $\Sigma NH_x$ include partitioning of $NH_3$ to smaller (e.g., recently

nucleated) particles than the size range captured by the AMS (70–1000 nm). $NH_3$ is not likely removed from plumes sampled in the upper boundary layer/free troposphere by deposition during our timescales of interest (e.g., Akagi et al., 2012), nor via oxidation by OH, given the lifetime of $NH_3$ against oxidation by OH is ~14 days ($k_{OH} = 1.6 \times 10^{-13}$ cm$^3$ molecule$^{-1}$ s$^{-1}$) (Sander et al., 2006).

$NH_3$ partitioning fractions in these plumes sampled during WE-CAN span a wide range. After 1.5 h, the plumes included here ranged from $pNH_4$ fractions of 0.2–0.9 ($pNH_4$ fraction = $pNH_4/\Sigma NH_x$). This is a wider range than described in the limited existing literature covering plumes that have been sampled as they age. For example, Akagi et al. (2012) observed a $pNH_4$ fraction of 0.13 after 1.5 h of aging in a southern California chaparral fire, and Yokelson et al. (2009) observed a $pNH_4$ fraction of ~0.32 after 1 h of aging in tropical Yucatán Peninsula smoke plumes.

We assume the loss of $NH_3$ from the gas-phase to follow a first order exponential decay toward a quasi-equilibrium value greater than zero. Our observations in older smoke show continued $NH_3$ enhancements (Figure S2a) and so an exponential decay toward 0 would not make sense, nor does it make sense from a thermodynamic point of view if $NH_4NO_3$ is present in the aerosol phase. Because we are fitting both an e-folding loss timescale as well as a quasi-equilibrium asymptote, our fits converge in only four out of the eight plumes. The estimated e-folding loss timescale of $NH_3$, $\tau_{NH3}$, in these four plumes is between ~24 and 4000 min (median of 55 min), with the Sharps Fire plume a possible outlier even though the fitting routine did converge. For comparison, Goode et al. (2000) observed an e-folding timescale of 2.5 h in aircraft observations of an Alaskan boreal fire plume, Akagi et al. (2012) estimated a lifetime of ~6 h after observing $NH_3$ normalized excess mixing ratios decreasing by 50% over 4.5 h of physical aging in aircraft measurements of a chaparral fire plume in California, and Adams et al. (2019) used IASI and CrIS satellite retrievals within 200 km of the Horse River wildfire in Canada to empirically estimate an $NH_3$ lifetime of 3 h. In wildfire smoke further from the fire source however, four studies have inferred longer first-order or effective lifetimes of $NH_3$: 36–48 h from correlation analysis of ground-based FTIR measurements (Lutsch et al., 2016); 6–24 h from regional analysis of IASI satellite retrievals over Russia (R'Honi et al., 2013); 36 h from a regional mass balance approach of IASI satellite retrievals over four tropical regions (Whitburn et al., 2015); and 21 h for an average effective lifetime in Indonesian peat fire plumes from IASI satellite retrievals (Whitburn et al., 2016). The differences between the shorter observed lifetimes in fresh smoke and the longer lifetimes inferred by the ground—and satellite-based regional analyses could be due to more abundant reactants for gas-particle partitioning reactions in fresh smoke (Paulot et al., 2017) as well as changing equilibrium conditions as the smoke dilutes and is advected downwind.

As Figure 3 shows, the Sharps Fire plume as sampled did not behave similarly to a gaussian-dispersing plume (with exponentially decaying CO enhancements). The flight scientist during that flight noted that at certain points it appeared as if smoke from a previous day of burning was being lifted out of the valley into the free troposphere. While we excluded transects with clear evidence of this influence from the current analysis, and the transects kept in meet the $t_0$ emission time criteria, the Sharps Fire plume likely represents an unideal case from which to estimate the timescale of gas-phase $NH_3$ loss. Timescales in the most well-defined plumes, Bear Trap first Pass and Taylor Creek, were estimated to be 120 ± 38 and 24 ± 54 min, respectively. The e-folding timescale of the average mixing ratio enhancements (i.e., not dilution corrected) of $NH_3$ and CO are shown in Figure 3. We observe e-folding timescales of $NH_3$ with respect to dilution plus chemical losses that range from 22 to 350 min (median of 77 min), generally shorter for a given plume than the timescales with respect to chemical losses only. E-folding distances range between 12 and 130 km (Figure S3) and could be useful in future satellite analyses and comparisons.

We also fit an asymptotic growth curve (the inverse of an exponential decay) to the $pNH_4$ NEMR estimates for each fire (Figure 2). The presence of $pNH_4$ in the downwind transect nearest to each fire suggests that a large fraction of the partitioning of gas-phase $NH_3$ into the aerosol happens on a timescale of tens of minutes between emission and the first *in situ* sampling transect. As we note above, the succeeding increase in $pNH_4$ is enough to balance the loss of gas-phase $NH_3$ within measurement errors for many fires. Over the short time span represented by these data (0–4 h of physical transport), in some cases (e.g., South Sugarloaf Fire Plume), $pNH_4$ NEMRs continue to increase as the plume ages, while in other cases the $pNH_4$ NEMR appears to stabilize. The e-folding timescales of the asymptotic growth in $pNH_4$ range from 17 to 180 min, with Bear Trap first Pass and Taylor Creek plumes estimates of 34 ± 50 and 17 ± 53 min, respectively.

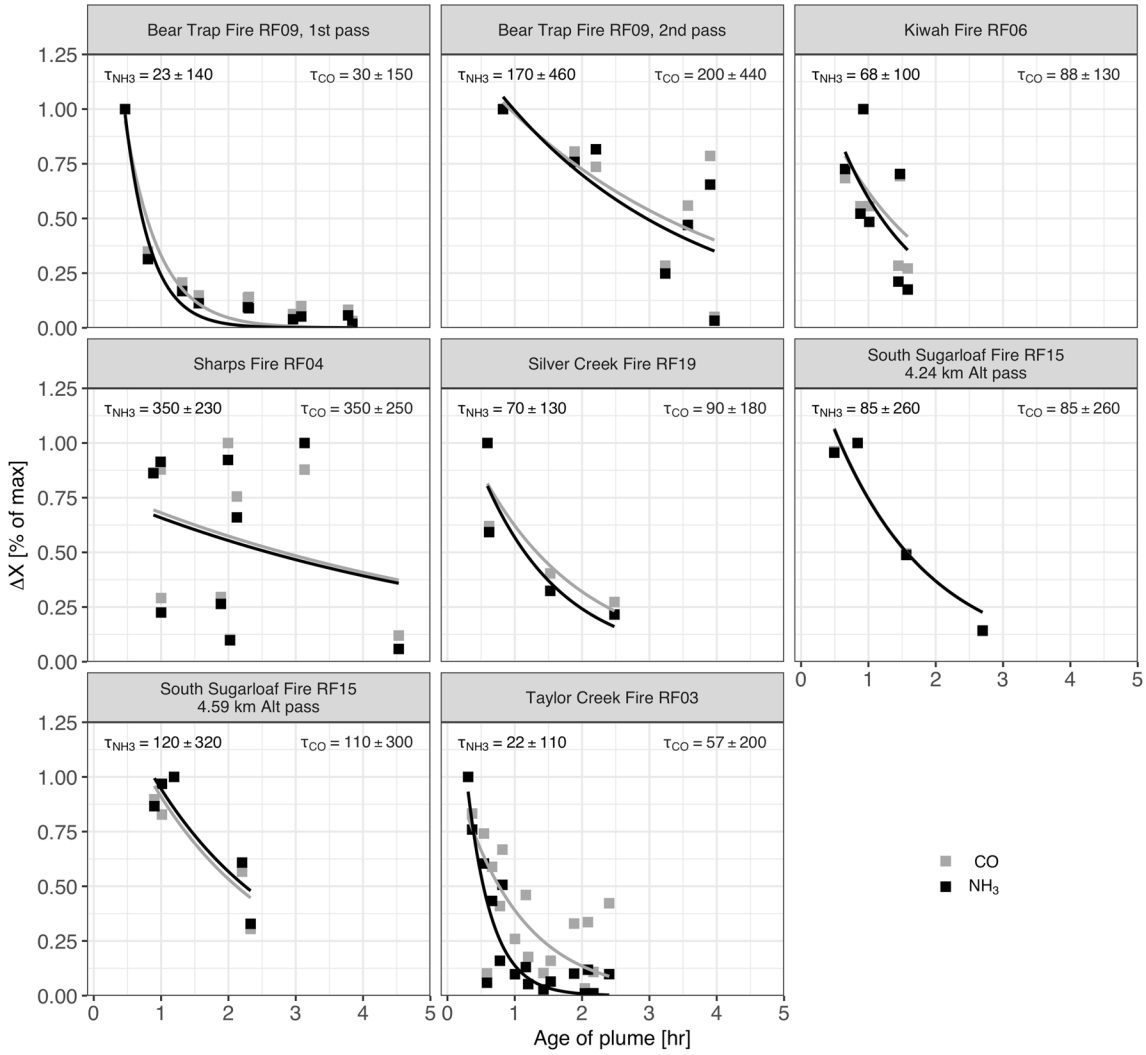


**Figure 3.** Evolution of ammonia ($NH_3$) and CO mixing ratios with estimated physical plume age. Points plotted are the mean mixing ratio of $NH_3$ in black and CO in gray of each plume transect, minus the estimated background and normalized by the greatest value across all passes in that plume (usually the youngest plume transect). $\tau_{NH3}$ represents the estimated e-folding time with respect to dilution + chemical losses with 1-sigma standard deviation in minutes, calculated for a first-order exponential decay to zero. $\tau_{CO}$ represents the estimated e-folding time with respect to dilution with 1-sigma standard deviation in minutes, again calculated for a first-order exponential decay to zero.

$NH_3$ partitioning to aerosol can end up in three forms. $NH_3$ can form inorganic salts with nitrate, sulphate, or other inorganic species (Seinfeld & Pandis, 2016). It can form salts with organic acids (Akagi et al., 2012; Malm et al., 2005; Schlag et al., 2017) or react with some organic compounds (e.g., some carbonyls) to form nitrogen-containing organic compounds (Laskin et al., 2015; Y. Liu et al., 2015; Updyke et al., 2012). It can also dissolve into solution and exist as an ammonium ion if a liquid phase exists in the aerosol (Seinfeld & Pandis, 2016). AMS $pNH_4$ should capture each of these forms, as well as reduced organic nitrogen such as amines, amides, and other N-containing molecules that fragment to ions attributed to $pNH_4$. Therefore, total $pNH_4$ may contain contributions from primary emissions of amines and other reduced N compounds, but these contributions to the observed increase in $pNH_4$ during pseudo-Lagrangian plume sampling are likely small since gas-phase amines and amides were measured at less than 5% of gas-phase $NH_3$ across all WE-CAN smoke plumes when they were intercepted (PTR-ToF-MS measurements; Lindaas et al., 2021).

If oxidized nitrogen chemistry is linked to (or indicative of) the partitioning of $NH_3$ to the aerosol through the formation of $NH_4NO_3$, we would expect a positive relationship between the fraction of $\Sigma NH_x$ that is $pNH_4$ and the fraction of the sum of measured oxidized nitrogen ($\Sigma NO_y$ = $NO_x$ + HONO + PAN + PPN

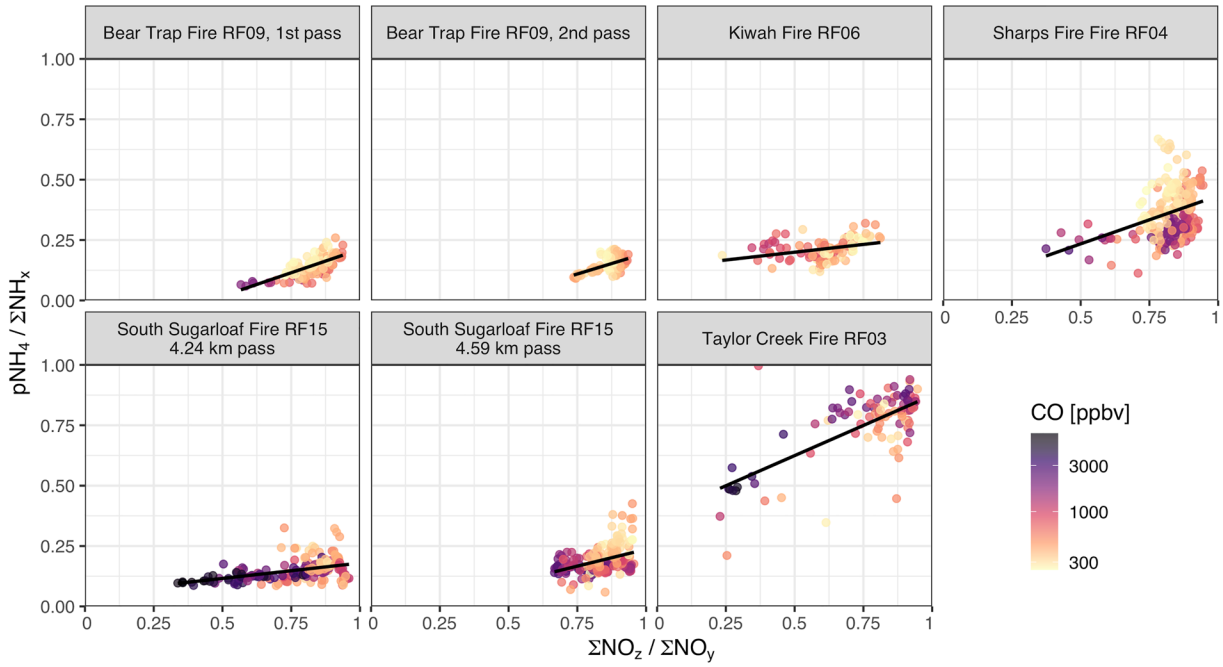


**Figure 4.** Relationship between the fraction of particulate ammonia ($p\mathrm{NH_4}$) out of total ammonia ($\Sigma\mathrm{NH_x} = \mathrm{NH_3} + p\mathrm{NH_4}$) and the fraction of more oxidized nitrogen species ($\Sigma\mathrm{NO_z} = \mathrm{PAN} + \mathrm{PPN} + \mathrm{HNO_3} + p\mathrm{NO_3} + \Sigma\mathrm{ONs}$) out of total reactive nitrogen oxides ($\Sigma\mathrm{NO_y} = \mathrm{NO_x} + \mathrm{HONO} + \mathrm{PAN} + \mathrm{PPN} + \mathrm{HNO_3} + p\mathrm{NO_3} + \Sigma\mathrm{ONs}$). All observations are averaged according to the 5 s timebase for measurements collected by the aerosal mass spectometer. Black lines represent linear least squares regression of the data points. Data points are colored by CO mixing ratio for all measurements above 250 ppbv.

+ $\mathrm{HNO_3}$ + $p\mathrm{NO_3}$ + ΣONs) that is NOz ($\Sigma\mathrm{NO_z}$ = PAN + PPN + $\mathrm{HNO_3}$ + $p\mathrm{NO_3}$ + ΣONs). This relationship is shown in Figure 4 for each plume where all data are available. Fresh plumes start with lower quantities of $p\mathrm{NH_4}/\Sigma\mathrm{NH_x}$ and $\Sigma\mathrm{NO_z}/\Sigma\mathrm{NO_y}$ and both quantities increase as the plume ages. The $\Sigma\mathrm{NO_z}/\Sigma\mathrm{NO_y}$ fraction is qualitatively similar to the negative log of $\mathrm{NO_x}$ fraction proxy for chemical age used in previous studies of wildfire smoke (e.g., Kleinman et al., 2008; Sedlacek III et al., 2018), and an increase in this fraction with aging reflects the transformation of $\mathrm{NO_x}$ into more highly oxidized products such as PAN, $\mathrm{HNO_3}$, and organic nitrates. As this chemistry proceeds, partitioning of $\mathrm{NH_3}$ into $p\mathrm{NH_4}$ is also occurring, whether via the formation of inorganic salts or through $\mathrm{NH_3}$–organic reactions. Figure 4 demonstrates three important patterns. First, for most plumes, $\Sigma\mathrm{NO_z}$ is more than 50% of $\Sigma\mathrm{NO_y}$. This is the case for even the first transect of the smoke plumes shown in Figure 4 and is a result of rapid oxidation of $\mathrm{NO_x}$ in the first tens of minutes after emission (Calahorrano et al., 2021; Peng et al., 2020). Second, the $p\mathrm{NH_4}$ fraction ranges widely between 0.1 and 0.9. The Taylor Creek Fire plume is an obvious outlier, with a $p\mathrm{NH_4}$ fraction~0.5 even in the freshest plume transects. There is evidence that Taylor Creek was a particularly chemically active plume, with high $\mathrm{NO_x}$ and HONO emission factors (Lindaas et al., 2021; Peng et al., 2020), the highest estimated $\mathrm{NO_x}$ relative to $\mathrm{NH_3}$ ($\mathrm{NO_x}/\mathrm{NH_3}$ ratio) of any fire (Lindaas et al., 2021), and more rapid $\mathrm{O_3}$ production than any other plume sampled. This plume is also unique with respect to the amount of aerosol sulphate ($p\mathrm{SO_4}$) relative to $\Sigma\mathrm{NH_x}$. In nearly all the fresh smoke plumes encountered during WE-CAN, Garofalo et al. (2019) show that there is more fine aerosol $p\mathrm{NH_4}$ and $p\mathrm{NO_3}$ mass than $p\mathrm{SO_4}$ mass. The exception is the plume associated with the Taylor Creek Fire. This is the only plume where the ratio of the total moles of $p\mathrm{SO_4}$ is greater than 10% of $\Sigma\mathrm{NH_x}$. We note that the timescale for gas-phase reaction of $\mathrm{SO_2}$ with OH oxidation to eventually form $p\mathrm{SO_4}$ is relatively slow (~2 days) compared to the timescales here (Long et al., 2017). Third, smaller CO mixing ratios at higher $p\mathrm{NH_4}$ fractions in the South Sugarloaf and Sharps Fire plumes suggest that under some circumstances more dilute smoke (either plume edges or physically older smoke) partitions a higher fraction of $\mathrm{NH_3}$ into the aerosol phase for a given fraction of $\mathrm{NO_z}$.

A companion manuscript by Calahorrano et al. (2021) estimates $\mathrm{HNO_3}$ formation from the OH oxidation of $\mathrm{NO_2}$ in the Bear Trap and Taylor Creek fire plumes. Assuming all produced $\mathrm{HNO_3}$ partitions to the aerosol

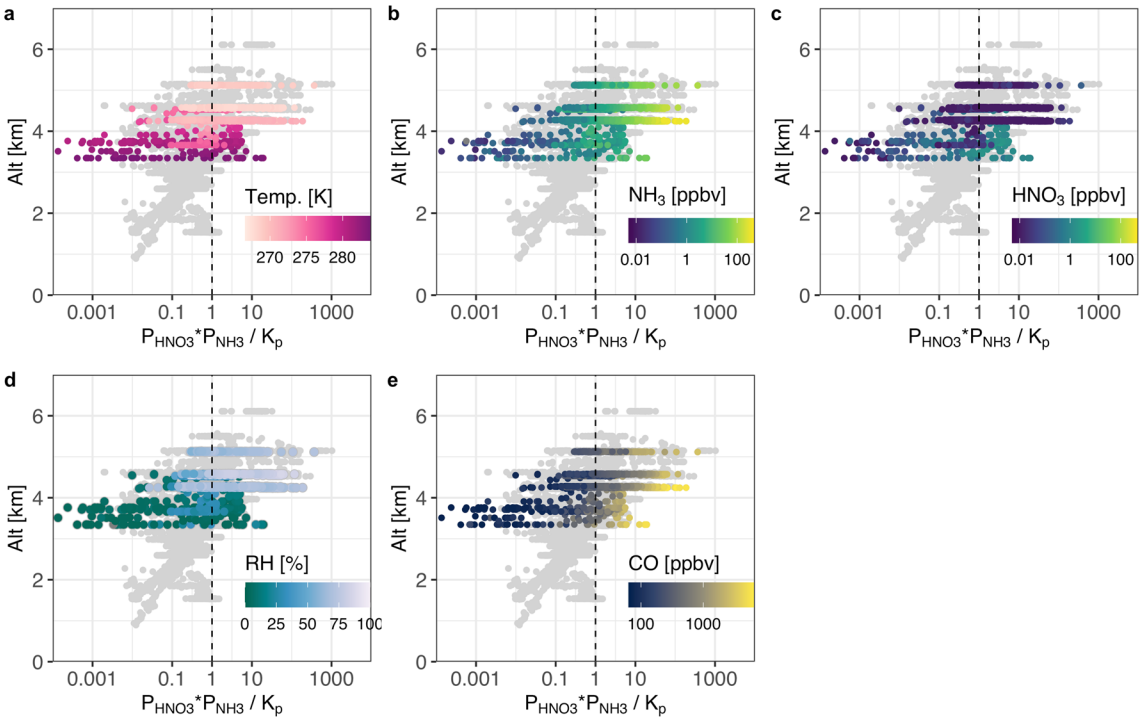


**Figure 5.** The altitude dependence of the ratio of the product of $NH_3$ and $HNO_3$ partial pressures with the dry dissociation constant for $NH_4NO_3$, $K_p$. All points are averaged measurements on the AMS timebase (5 s). Gray points show all measurements within identified smoke plumes throughout the campaign. Colored points are those from the eight fire plumes included in prior figures. Each panel is colored by a different measurement: (a) ambient temperature, (b) $NH_3$ mixing ratio, (c) $HNO_3$ mixing ratio, (d) ambient relative humidity, and (e) CO mixing ratio. The vertical dashed line in each panel indicates a $K_p$ ratio of 1.

phase in association with $NH_3$, they find that $NO_2$ oxidation by OH can account for ~100% of the $pNO_3$ formation in the Taylor Creek plume, and ~300% of the $pNO_3$ formation in Bear Trap. Possible reasons for the overestimation of $pNO_3$ increases could include an incomplete understanding of OH concentration evolution and uptake of $HNO_3$ by super-micron particles. These rough estimates support the conclusion that the partitioning of $NH_3$ into the aerosol phase is at least in part due to the formation of $NH_4NO_3$ through the association with gas-phase $HNO_3$.

To investigate the thermodynamics of possible $NH_4NO_3$ formation within WE-CAN smoke plumes, we calculate the dissociation constant of $NH_4NO_3$, $K_p$ (Table 10.7 in Seinfeld & Pandis, 2016), and compare it to the product of partial pressures of gas-phase $NH_3$ and $HNO_3$ (Figure 5). $K_p$ is dependent on temperature (Figure 5a) (see also Stelson & Seinfeld, 1982), and it indicates whether a parcel is supersaturated with respect to $NH_4NO_3$ when particles are dry (which assumes a low environmental relative humidity and particles have not deliquesced). This $K_p$ formulation does not consider physical and chemical properties of the smoke aerosol that may shift particles away from $NH_4NO_3$ equilibrium such as mixing state, phase separation, and aerosol pH (e.g., Guo et al., 2018; Kanakidou et al., 2005). Higher relative humidities (typically > 60%) will likely cause $NH_4NO_3^-$containing aerosol to deliquesce at the temperatures sampled here, increasing the likelihood of additional $NH_4NO_3$ formation. 63% of samples had RH <60% in the data shown in Figure 5d, but for simplicity we always assume the aerosol is dry. When the product of $NH_3$ and $HNO_3$ partial pressures is greater than $K_p$, or a ratio >1 (vertical dashed lines in Figure 5), the parcel is assumed to be $NH_4NO_3$ supersaturated, and $NH_4NO_3$ will form as the system moves toward thermodynamic equilibrium. Conversely a $K_p$ ratio <1 indicates the parcel is $NH_4NO_3$ subsaturated and $NH_4NO_3$ in aerosol, if it exists, will start to dissociate and transition back into the gas-phase as the system moves toward equilibrium.

Figure 5 shows that $NH_4NO_3$ supersaturation (points to the right of the vertical dashed lines) is more likely in higher altitude plumes because the temperature dependence of $K_p$ pushes partitioning of $NH_4NO_3$ toward the particle phase, as inferred by Paulot et al. (2017). Individual data points in the plumes sampled during WE-CAN span a wide range of $K_p$ ratios, from 0.001 to 1,000; low values are driven by low $NH_3$ and

$HNO_3$ mixing ratios and warmer temperatures (Figures 5a–5c), and high values are driven by high $NH_3$ mixing ratios and colder temperatures. The total amount of available $NH_3$ and $HNO_3$ drives the relative amount of possible $NH_4NO_3$ formed, assuming there are no other physical or chemical constraints to the systems' equilibrium, and under this assumption the large range of observed $K_p$ ratios indicates that the smoke is not often near $NH_4NO_3$ equilibrium. It is possible these observations of $K_p$ ratios far out of equilibrium could constitute evidence for the influence of different physical and chemical properties mentioned above. Garofalo et al. (2019) showed that sub-micron aerosol measured during WE-CAN were generally > 85% organic, and thus it is likely many bulk properties are dominated by organic compounds.

$NH_3$ is nearly always in excess in these plumes, particularly when the $K_p$ ratio is >1, and thus $HNO_3$ may be a limiting factor in the formation of $NH_4NO_3$ (Figures 5b and 5c). Gas-phase $HNO_3$ enhancements were not observed or they were small (typically < 5 ppbv; Figure S2b) compared to tens or hundreds of ppbv in observed $NH_3$ mixing ratios (Figure S2a), implying that $NH_4NO_3$ formation is $HNO_3$ limited. $NH_4NO_3$ supersaturation is also more common in fresher denser plumes (Figure 5e), where appreciable quantities of $HNO_3$ have sometimes been produced (Figure 5c) and before dilution reduces the total abundances of both $NH_3$ and $HNO_3$.

As stated earlier, the $pNH_4$ measurement in smoke may contain contributions from inorganic $NH_4^+$ as salts with either inorganic acid anions (i.e., $NH_4^+$ associated with $NO_3^-$ or $SO_4^{2-}$) or with organic acids (e.g., Akagi et al., 2012). Additionally, the $pNH_4$ measurement includes reduced organic N such as amines or other covalently bonded reduced organic nitrogen compounds (e.g., Farmer et al., 2010; Lin et al., 2016). Thus, not all of the $pNH_4$ measured in smoke is necessarily inorganic, and not all of the inorganic $pNH_4$ is necessarily in salts with inorganic acids. We note that organic acid ions from the PILS measurements (formate, acetate, oxalate, malonate, succinate, and glutarate) are present in the WE-CAN data set. The formation of organic $NH_4$ salts would be consistent with previously observed enrichment of organic acids and $NH_4^+$ observed in boreal forest fire smoke (Talbot et al., 1992) and tropical Amazon biomass burning haze (Andreae et al., 1988), though we note that smoke in these studies was estimated to be older than the fresh smoke measurements analyzed here. Though outside the scope of this analysis, further work is needed to estimate the fraction of inorganic versus organic NH4 salts, as well as to investigate the possibility of covalently bonded reduced N to the $pNH_4$ measurement. Empirical AMS species apportioning analyses for $pNH_4$ during WE-CAN are ongoing.

While Figure 5 shows the physical and chemical context for $NH_4NO_3$ thermodynamic equilibrium in smoke connected to a specific fire and with a physical age of <1 day, we also encountered smoke of indeterminate origin, some of which had likely been emitted more than 1 day prior to sampling. Though establishing an estimated physical age is difficult for this smoke, we can use estimated chemical age categories described by O'Dell et al. (2020) to assess how the physical smoke context may change the $pNH_4$ fraction ($pNH_4/\Sigma NH_x$) in older smoke. The first three panels in Figure 6 shows that there is a negative correlation between the ambient environmental temperature and the $pNH_4$ fraction in medium (1–3 days chemical aging) and old (>3 days chemical aging) smoke, while this relationship is not present in the young smoke (<1 day chemical aging). We note that most of the data previously presented in Figures 2–5 is classified as young smoke. Temperature here can be considered an inverse proxy for altitude, with higher sampling altitudes typically having lower temperatures. As might be expected, relative humidity is also correlated with $pNH_4$ fraction in medium and old smoke, meaning higher $pNH_4$ fractions are observed at both colder temperatures and higher relative humidities (Figure S4). Since colder and wetter conditions push the $NH_4NO_3$ equilibrium toward the aerosol-phase, these empirical relationships suggest a larger contribution from inorganic $NH_3$ partitioning in colder and wetter smoke plumes. Figures 6e and 6f support this conclusion, showing the same negative relationship with temperature for the fraction of $pNO_3$ in the sum measured nitrate ($\Sigma NO_3 = pNO_3 + HNO_3$) in medium and old smoke. This conclusion is also consistent with the inference made by Paulot et al. (2017), that smoke plumes injected higher into the free troposphere more favorably produce $NH_4NO_3$. The fractions of $pNH_4$ and $pNO_3$ in each of the Figure 6 panels are colored by the ratio of measured sum nitrate to measured sum ammonia ($\Sigma NO_3/\Sigma NH_x$). This ratio suggests that a greater abundance of sum nitrate relative to sum ammonia is correlated with a higher $pNH_4$ fraction in young and medium chemically aged smoke. Higher $\Sigma NO_3/\Sigma NH_x$ correlating with greater $NH_3$ partitioning is consistent with one of the insights from Figure 5, that $NH_4NO_3$ production is often limited by $HNO_3$ availability,

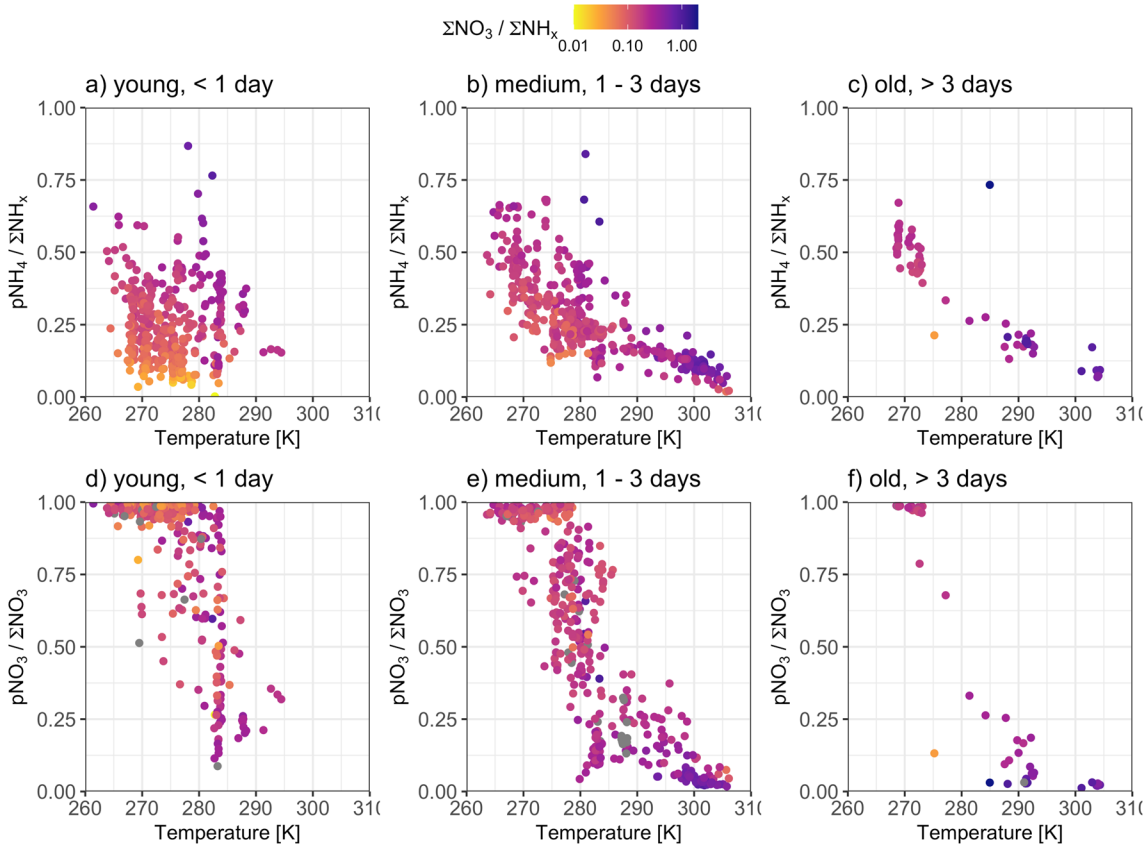


**Figure 6.** (a–c) Measured $p\mathrm{NH_4}$ fraction ($p\mathrm{NH_4}/\Sigma\mathrm{NH_x}$) as a function of temperature, binned by young, medium, and old smoke, as defined by chemical age estimates from (O'Dell et al., 2020). (d–f) Measured $p\mathrm{NO_3}$ fraction ($p\mathrm{NO_3}/\Sigma\mathrm{NO_3}$; $\Sigma\mathrm{NO_3} = p\mathrm{NO_3} + \mathrm{HNO_3}$) as a function of temperature, binned by the same chemical age estimates. Observations are averaged to the timebase of the TOGA instrument (~30-s samples every 100 s) and colored by the ratio of measured sum nitrate to measured sum ammonia ($\Sigma\mathrm{NO_3}/\Sigma\mathrm{NH_x}$) on a $\log_{10}$ scale. Data points include only the observations collected >2 km above sea level in order to limit ground-based emission influence, and are not background-corrected.

as well as the observations from individual fires, where Taylor Creek has the fastest e-folding loss timescale and the highest oxidized N to reduced N ratios (Lindaas et al., 2021). We note that the data shown in Figure 6 are not background-corrected, thus describing the behavior of total ammonia (panels a–c) and total nitrate (panels d–f) in smoke-impacted air. While entrainment of $\mathrm{NH_3}$, $p\mathrm{NH_4}$, and $p\mathrm{NO_3}$ from surrounding air masses is not likely to be contribute to already enhanced abundances in older smoke, $\mathrm{HNO_3}$ may be present in the free troposphere (Figure S2b) and affect the $p\mathrm{NO_3}$ fraction in well-diluted (medium and old) smoke along with smoke-produced $\mathrm{HNO_3}$. By showing the full observed behavior of the $p\mathrm{NH_4}$ and $p\mathrm{NO_3}$ fractions in smoke across different chemical ages, we conclude that aged smoke plumes in the western U.S. likely contribute to the production of $\mathrm{NH_4NO_3}$ in the free troposphere. This production may be enhanced in smoke with lower temperatures (injection at higher altitudes) and higher $\Sigma\mathrm{NO_3}/\Sigma\mathrm{NH_x}$ ratios.

## 4. Conclusions

We have characterized evolution of gas-phase $\mathrm{NH_3}$ in a set of western wildfire smoke plumes during summer 2018 and investigated some of the complexity in the partitioning of $\mathrm{NH_3}$ to $p\mathrm{NH_4}$, including the relationship of $\mathrm{NH_3}$ partitioning to $\mathrm{HNO_3}$ and other acids as well as to temperature and RH. $\mathrm{NH_3}$ mixing ratios decrease in fresh smoke plumes in most of the sampled plumes, faster than can be explained by dilution alone, and concurrent increases in observed sub-micron $p\mathrm{NH_4}$ from the AMS are able to account for this loss in many plumes. While the limited existing literature on $\mathrm{NH_3}$ evolution in smoke tends to estimate a lifetime or effective lifetime for $\mathrm{NH_3}$ loss, we recognize the complexity in this term: $\mathrm{NH_3}$ is likely lost from the gas phase through an equilibrium process dependant on $T$ and RH that happens concurrent with ongoing dilution

and changing inorganic and organic acids abundances. Thus, we describe an e-folding loss timescale to quasi-equilibrium for $NH_3$ gas-particle partitioning that is on the order of tens of minutes to several hours in the fresh smoke plumes sampled. We find empirical evidence for the association of $NH_3$ and $HNO_3$ to form $NH_4NO_3$ through the positive relationship between the $pNH_4$ fraction of $\Sigma NH_x$ and the $\Sigma NO_z$ fraction of $\Sigma NO_y$. We examine the thermodynamic context for the formation of $NH_4NO_3$ by calculating the $K_p$ ratio. Under the assumption that this equilibrium is independent from aerosol mixing state, phase separation, or pH, we find that many of our *in situ* measurements are far from equilibrium, both super- and sub-saturated with respect to $NH_4NO_3$. Fresh, dense plumes injected at higher altitudes (and lower temperatures) are more likely to favor $NH_4NO_3$ formation. Lastly, in smoke with chemical ages older than ~1 day, we find evidence for the presence of $NH_4NO_3$ via the negative relationship between the environmental temperature and both $pNH_4$ and $pNO_3$ fractions. This again suggests that smoke injected higher in the free troposphere favors the formation of $NH_4NO_3$, consistent with the findings of Paulot et al. (2017).

There is a need for more *in situ* observations of $NH_3$ evolution, not only in this region but also for boreal and tropical regions. Fires in these regions can have very different emission ratios of reactive nitrogen species (e.g., Akagi et al., 2011). This study concurs with expectations that larger emission ratios of $NO_x/NH_3$ produce faster $NH_3$ partitioning via formation of $NH_4NO_3$. Additional *in situ* observations could help confirm partitioning rates under real-world conditions. Additionally, there is a need for *in situ* and satellite analyses that bridge the first few hours of physical aging with the evolution that occurs over the first few days of atmospheric transport, including nighttime chemical processes. Subsequent smoke-centered field projects or opportunistic smoke sampling efforts might include this focus in their data collection and analyses.

## Conflict of Interest

The authors declare no conflicts of interest.

## Data Availability Statement

All data are available in the WE-CAN data archive (https://data.eol.ucar.edu/master_lists/generated/we-can/).

**Acknowledgments**
Funding for this work was provided by the US National Science Foundation (NSF award numbers: AGS-1650786, AGS-1650275, AGS-1950327, and AGS-1652688) and the US National Oceanic and Atmospheric Administration (NOAA) under award numbers NA17OAR4310010 and NA17OAR4310001.

## References

Adams, C., McLinden, C. A., Shephard, M. W., Dickson, N., Dammers, E., Chen, J., et al. (2019). Satellite-derived emissions of carbon monoxide, ammonia, and nitrogen dioxide from the 2016 Horse River wildfire in the Fort McMurray area. *Atmospheric Chemistry and Physics*, *19*(4), 2577–2599. https://doi.org/10.5194/acp-19-2577-2019

Akagi, S. K., Craven, J. S., Taylor, J. W., McMeeking, G. R., Yokelson, R. J., Burling, I. R., et al. (2012). Evolution of trace gases and particles emitted by a chaparral fire in California. *Atmospheric Chemistry and Physics*, *12*(3), 1397–1421. https://doi.org/10.5194/acp-12-1397-2012

Akagi, S. K., Yokelson, R. J., Wiedinmyer, C., Alvarado, M. J., Reid, J. S., Karl, T., et al. (2011). Emission factors for open and domestic biomass burning for use in atmospheric models. *Atmospheric Chemistry and Physics*, *11*(9), 4039–4072. https://doi.org/10.5194/acp-11-4039-2011

Alvarado, M. J., Logan, J. A., Mao, J., Apel, E., Riemer, D., Blake, D., et al. (2010). Nitrogen oxides and PAN in plumes from boreal fires during ARCTAS-B and their impact on ozone: An integrated analysis of aircraft and satellite observations. *Atmospheric Chemistry and Physics*, *10*(20), 9739–9760. https://doi.org/10.5194/acp-10-9739-2010

Andreae, M. O., Browell, E. V., Garstang, M., Gregory, G. L., Harriss, R. C., Hill, G. F., et al. (1988). Biomass-burning emissions and associated haze layers over Amazonia. *Journal of Geophysical Research*, *93*(D2), 1509–1527. https://doi.org/10.1029/jd093id02p01509

Aschmann, S. M., Nishino, N., Arey, J., & Atkinson, R. (2011). Kinetics of the reactions of OH radicals with 2- and 3-methylfuran, 2,3- and 2,5-dimethylfuran, and E- and Z-3-hexene-2,5-dione, and products of OH + 2,5-dimethylfuran. *Environmental Science & Technology*, *45*(5), 1859–1865. https://doi.org/10.1021/es103207k

Atkinson, R. (1986). Kinetics and mechanisms of the gas-phase reactions of the hydroxyl radical with organic compounds under atmospheric conditions. *Chemical Reviews*, *86*(1), 69–201. https://doi.org/10.1021/cr00071a004

Behera, S. N., & Sharma, M. (2010). Investigating the potential role of ammonia in ion chemistry of fine particulate matter formation for an urban environment. *Science of the Total Environment*, *408*(17), 3569–3575. https://doi.org/10.1016/j.scitotenv.2010.04.017

Benedict, K. B., Prenni, A. J., Carrico, C. M., Sullivan, A. P., Schichtel, B. A., & Collett, J. L. (2017). Enhanced concentrations of reactive nitrogen species in wildfire smoke. *Atmospheric Environment*, *148*, 8–15. https://doi.org/10.1016/j.atmosenv.2016.10.030

Bouwman, A. F., Lee, D. S., Asman, W. A. H., Dentener, F. J., Hoek, K. W. V. D., & Olivier, J. G. J. (1997). A global high-resolution emission inventory for ammonia. *Global Biogeochemical Cycles*, *11*(4), 561–587. https://doi.org/10.1029/97gb02266

Bray, C. D., Battye, W., Aneja, V. P., Tong, D. Q., Lee, P., & Tang, Y. (2018). Ammonia emissions from biomass burning in the continental United States. *Atmospheric Environment*, *187*, 50–61. https://doi.org/10.1016/j.atmosenv.2018.05.052

Calahorrano, J. F. J., Lindaas, J., O'Dell, K., Palm, B. B., Peng, Q., Flocke, F., et al. (2021). Daytime oxidized reactive nitrogen partitioning in Western U.S. Wildfire smoke plumes. *Journal of Geophysical Research: Atmosphere*, *126*(4), e2020JD033484. https://doi.org/10.1029/2020jd033484

Chen, X., Day, D., Schichtel, B., Malm, W., Matzoll, A. K., Mojica, J., et al. (2014). Seasonal ambient ammonia and ammonium concentrations in a pilot IMPROVE NHx monitoring network in the western United States. *Atmospheric Environment*, *91*, 118–126. https://doi.org/10.1016/j.atmosenv.2014.03.058

Collier, S., Zhou, S., Onasch, T. B., Jaffe, D. A., Kleinman, L., Sedlacek, A. J., et al. (2016). Regional influence of Aerosol emissions from wildfires driven by combustion efficiency: Insights from the BBOP Campaign. *Environmental Science & Technology*, *50*(16), 8613–8622. https://doi.org/10.1021/acs.est.6b01617

Dammers, E., McLinden, C. A., Griffin, D., Shephard, M. W., Graaf, S. V. D., Lutsch, E., et al. (2019). $NH_3$ emissions from large point sources derived from CrIS and IASI satellite observations. *Atmospheric Chemistry and Physics*, *19*(19), 12261–12293. https://doi.org/10.5194/acp-19-12261-2019

Farmer, D. K., Matsunaga, A., Docherty, K. S., Surratt, J. D., Seinfeld, J. H., Ziemann, P. J., & Jimenez, J. L. (2010). Response of an aerosol mass spectrometer to organonitrates and organosulfates and implications for atmospheric chemistry. *Proceedings of the National Academy of Sciences*, *107*(15), 6670–6675. https://doi.org/10.1073/pnas.0912340107

Garofalo, L. A., Pothier, M. A., Levin, E. J. T., Campos, T., Kreidenweis, S. M., & Farmer, D. K. (2019). Emission and evolution of submicron organic Aerosol in smoke from wildfires in the Western United States. *ACS Earth and Space Chemistry*, *3*(7), 1237–1247. https://doi.org/10.1021/acsearthspacechem.9b00125

Goode, J. G., Yokelson, R. J., Ward, D. E., Susott, R. A., Babbitt, R. E., Davies, M. A., & Hao, W. M. (2000). Measurements of excess $O_3$, $CO_2$, CO, $CH_4$, $C_2H_4$, $C_2H_2$, HCN, NO, $NH_3$, HCOOH, $CH_3COOH$, HCHO, and $CH_3OH$ in 1997 Alaskan biomass burning plumes by airborne Fourier transform infrared spectroscopy (AFTIR). *Journal of Geophysical Research*, *105*(D17), 22147–22166. https://doi.org/10.1029/2000jd900287

Guo, H., Otjes, R., Schlag, P., Kiendler-Scharr, A., Nenes, A., & Weber, R. J. (2018). Effectiveness of ammonia reduction on control of fine particle nitrate. *Atmospheric Chemistry and Physics*, *18*(16), 12241–12256. https://doi.org/10.5194/acp-18-12241-2018

Harris, G. W., Kleindienst, T. E., & Pitts, J. N. (1981). Rate constants for the reaction of OH radicals with CH3CN, C2H5CN AND CH2=CH-CN in the temperature range 298–424 K. *Chemical Physics Letters*, *80*(3), 479–483. https://doi.org/10.1016/0009-2614(81)85061-0

Hecobian, A., Liu, Z., Hennigan, C. J., Huey, L. G., Jimenez, J. L., Cubison, M. J., et al. (2011). Comparison of chemical characteristics of 495 biomass burning plumes intercepted by the NASA DC-8 aircraft during the ARCTAS/CARB-2008 field campaign. *Atmospheric Chemistry and Physics*, *11*(24), 13325–13337. https://doi.org/10.5194/acp-11-13325-2011

Hobbs, P. V., Sinha, P., Yokelson, R. J., Christian, T. J., Blake, D. R., Gao, S., et al. (2003). Evolution of gases and particles from a savanna fire in South Africa: Evolution of gases and particles. *Journal of Geophysical Research*, *108*(D13). https://doi.org/10.1029/2002jd002352

Holloway, T., Levy, H., & Kasibhatla, P. (2000). Global distribution of carbon monoxide. *Journal of Geophysical Research*, *105*(D10), 12123–12147. https://doi.org/10.1029/1999jd901173

Kanakidou, M., Seinfeld, J. H., Pandis, S. N., Barnes, I., Dentener, F. J., Facchini, M. C., et al. (2005). Organic aerosol and global climate modelling: A review. *Atmospheric Chemistry and Physics*, *5*(4), 1053–1123. https://doi.org/10.5194/acp-5-1053-2005

Karlsson, P. E., Ferm, M., Tømmervik, H., Hole, L. R., Pihl Karlsson, G., Ruoho-Airola, T., et al. (2013). Biomass burning in eastern Europe during spring 2006 caused high deposition of ammonium in northern Fennoscandia. *Environmental Pollution*, *176*, 71–79. https://doi.org/10.1016/j.envpol.2012.12.006

Kleinman, L. I., Springston, S. R., Daum, P. H., Weinstein-Lloyd, J., Alexander, M. L., Hubbe, J., et al. (2008). The time evolution of aerosol composition over the Mexico City plateau. *Atmospheric Chemistry and Physics*, *17*, 1559–1575. https://doi.org/10.5194/acp-8-1559-2008

Laskin, A., Laskin, J., & Nizkorodov, S. A. (2015). Chemistry of atmospheric brown carbon. *Chemical Reviews*, *115*(10), 4335–4382. https://doi.org/10.1021/cr5006167

Li, Q., Jacob, D. J., Bey, I., Yantosca, R. M., Zhao, Y., Kondo, Y., & Notholt, J. (2000). Atmospheric hydrogen cyanide (HCN): Biomass burning source, ocean sink? *Geophysical Research Letters*, *27*(3), 357–360. https://doi.org/10.1029/1999gl010935

Lin, P., Aiona, P. K., Li, Y., Shiraiwa, M., Laskin, J., Nizkorodov, S. A., & Laskin, A. (2016). Molecular characterization of brown carbon in biomass burning aerosol particles. *Environmental Science & Technology*, *50*(21), 11815–11824. https://doi.org/10.1021/acs.est.6b03024

Lindaas, J., Pollack, I. B., Garofalo, L. A., Pothier, M. A., Farmer, D. K., Kreidenweis, S. M., et al. (2021). Emissions of reactive nitrogen from Western U.S. Wildfires during summer 2018. *Journal of Geophysical Research: Atmosphere*, *126*(2), e2020JD032657. https://doi.org/10.1029/2020jd032657

Liu, X., Zhang, Y., Huey, L. G., Yokelson, R. J., Wang, Y., Jimenez, J. L., et al. (2016). Agricultural fires in the southeastern U.S. during SEAC4RS: Emissions of trace gases and particles and evolution of ozone, reactive nitrogen, and organic aerosol. *Journal of Geophysical Research: Atmosphere*, *121*(12), 7383–7414. https://doi.org/10.1002/2016jd025040

Liu, Y., Liggio, J., Staebler, R., & Li, S.-M. (2015). Reactive uptake of ammonia to secondary organic aerosols: Kinetics of organonitrogen formation. *Atmospheric Chemistry and Physics*, *15*(23), 13569–13584. https://doi.org/10.5194/acp-15-13569-2015

Long, B., Bao, J. L., & Truhlar, D. G. (2017). Reaction of $SO_2$ with OH in the atmosphere. *Physical Chemistry Chemical Physics*, *19*(11), 8091–8100. https://doi.org/10.1039/C7CP00497D

Lutsch, E., Dammers, E., Conway, S., & Strong, K. (2016). Long-range transport of NH3, CO, HCN, and C2H6 from the 2014 Canadian Wildfires. *Geophysical Research Letters*, *43*(15), 8286–8297. https://doi.org/10.1002/2016gl070114

Malm, W. C., Day, D. E., Carrico, C., Kreidenweis, S. M., Collett, J. L., McMeeking, G., et al. (2005). Intercomparison and closure calculations using measurements of aerosol species and optical properties during the Yosemite Aerosol Characterization Study. *Journal of Geophysical Research*, *110*(D14). https://doi.org/10.1029/2004jd005494

Myhre, G., Shindell, D., Bréon, F.-M., Collins, W., Fuglestvedt, J., Huang, J., & Shine, K. (2013). *Anthropogenic and natural radiative forcing (tech. Rep.)*. Cambridge University Press.

O'Dell, K., Hornbrook, R. S., Permar, W., Levin, E. J. T., Garofalo, L. A., Apel, E. C., et al. (2020). Hazardous air pollutants in fresh and aged Western US wildfire smoke and implications for long-term exposure. *Environmental Science & Technology*, *54*(19), 11838–11847. https://doi.org/10.1021/acs.est.0c04497

Paulot, F., Jacob, D. J., Pinder, R. W., Bash, J. O., Travis, K., & Henze, D. K. (2014). Ammonia emissions in the United States, European Union, and China derived by high-resolution inversion of ammonium wet deposition data: Interpretation with a new agricultural emissions inventory (MASAGE_nh3). *Journal of Geophysical Research: Atmosphere*, *119*(7), 4343–4364. https://doi.org/10.1002/2013jd021130

Paulot, F., Paynter, D., Ginoux, P., Naik, V., Whitburn, S., Damme, M. V., et al. (2017). Gas-aerosol partitioning of ammonia in biomass burning plumes: Implications for the interpretation of spaceborne observations of ammonia and the radiative forcing of ammonium nitrate. *Geophysical Research Letters*, *44*(15), 8084–8093. https://doi.org/10.1002/2017gl074215

Peng, Q., Palm, B. B., Melander, K. E., Lee, B. H., Hall, S. R., Ullmann, K., et al. (2020).HONO emissions from Western U.S. Wildfires provide dominant radical source in fresh wildfire smoke. *Environmental Science & Technology*, *54*(10), 5954–5963. https://doi.org/10.1021/acs.est.0c00126

Pollack, I. B., Lindaas, J., Roscioli, J. R., Agnese, M., Permar, W., Hu, L., & Fischer, E. V. (2019). Evaluation of ambient ammonia measurements from a research aircraft using a closed-path QC-TILDAS operated with active continuous passivation. *Atmospheric Measurement Techniques*, *12*(7), 3717–3742. https://doi.org/10.5194/amt-12-3717-2019

Prenni, A. J., Levin, E. J. T., Benedict, K. B., Sullivan, A. P., Schurman, M. I., Gebhart, K. A., et al. (2014). Gas-phase reactive nitrogen near Grand Teton National Park: Impacts of transport, anthropogenic emissions, and biomass burning. *Atmospheric Environment*, *89*, 749–756. https://doi.org/10.1016/j.atmosenv.2014.03.017

R'Honi, Y., Clarisse, L., Clerbaux, C., Hurtmans, D., Duflot, V., Turquety, S., et al. (2013). Exceptional emissions of $NH_3$ and HCOOH in the 2010 Russian wildfires. *Atmospheric Chemistry and Physics*, *13*(8), 4171–4181. https://doi.org/10.5194/acp-13-4171-2013

Roberts, J. M., Stockwell, C. E., Yokelson, R. J., Gouw, J. D., Liu, Y., Selimovic, V., et al. (2020). The nitrogen budget of laboratory-simulated western U.S. wildfires during the FIREX 2016 FireLab study. *Atmospheric Chemistry and Physics Discussions*, *1–34*. https://doi.org/10.5194/acp-2020-66

Sander, S. P., Golden, D. M., Kurylo, M. J., Moortgat, G. K., Wine, P. H., Ravishankara, A. R., et al. (2006). *Chemical kinetics and photochemical data for use in atmospheric studies: Evaluation number 15 (Technical Report)*. Jet Propulsion Laboratory, California Institute of Technology.

Schlag, P., Rubach, F., Mentel, T. F., Reimer, D., Canonaco, F., Henzing, J. S., et al. (2017). Ambient and laboratory observations of organic ammonium salts in PM1. *Faraday Discussions*, *200*(0), 331–351. https://doi.org/10.1039/C7FD00027H

Sedlacek, III A. J., Buseck, P. R., Adachi, K., Onasch, T. B., Springston, S. R., & Kleinman, L. (2018). Formation and evolution of tar balls from northwestern US wildfires. *Atmospheric Chemistry and Physics*, *18*(15), 11289–11301. https://doi.org/10.5194/acp-18-11289-2018

Seinfeld, J. H., & Pandis, S. N. (2016). *Atmospheric chemistry and physics: From air pollution to climate change*, 3rd ed. Wiley.

Song, C. H., Ma, Y., Orsini, D., Kim, Y. P., & Weber, R. J. (2005). An investigation into the ionic chemical composition and mixing state of biomass burning particles recorded during TRACE-P P3B Flight#10. *Journal of Atmospheric Chemistry*, *51*(1), 43–64. https://doi.org/10.1007/s10874-005-5727-9

Stelson, A. W., & Seinfeld, J. H. (1982). Relative humidity and temperature dependence of the ammonium nitrate dissociation constant. *Atmospheric Environment*, *16*(5), 983–992. https://doi.org/10.1016/0004-6981(82)90184-6

Talbot, R. W., Vijgen, A. S., & Harriss, R. C. (1992). Soluble species in the Arctic summer troposphere: Acidic gases, aerosols, and precipitation. *Journal of Geophysical Research: Atmosphere*, *97*(D15), 16531–16543. https://doi.org/10.1029/91jd00118

Updyke, K. M., Nguyen, T. B., & Nizkorodov, S. A. (2012). Formation of brown carbon via reactions of ammonia with secondary organic aerosols from biogenic and anthropogenic precursors. *Atmospheric Environment*, *63*, 22–31. https://doi.org/10.1016/j.atmosenv.2012.09.012

Whitburn, S., Damme, M. V., Clarisse, L., Turquety, S., Clerbaux, C., & Coheur, P.-F. (2016). Doubling of annual ammonia emissions from the peat fires in Indonesia during the 2015 El Niño. *Geophysical Research Letters*, *43*(20), 11007–11014. https://doi.org/10.1002/2016gl070620

Whitburn, S., Damme, M.V., Kaiser, J. W., van der Werf, G. R., Turquety, S., Hurtmans, D., et al. (2015). Ammonia emissions in tropical biomass burning regions: Comparison between satellite-derived emissions and bottom-up fire inventories. *Atmospheric Environment*, *121*, 42–54. https://doi.org/10.1016/j.atmosenv.2015.03.015

Yokelson, R. J., Andreae, M. O., & Akagi, S. K. (2013). Pitfalls with the use of enhancement ratios or normalized excess mixing ratios measured in plumes to characterize pollution sources and aging. *Atmospheric Measurement Techniques*, *6*(8), 2155–2158. https://doi.org/10.5194/amt-6-2155-2013

Yokelson, R. J., Crounse, J. D., DeCarlo, P. F., Karl, T., Urbanski, S., Atlas, E., et al. (2009). Emissions from biomass burning in the Yucatan. *Atmospheric Chemistry and Physics*, *9*(15), 5785–5812. https://doi.org/10.5194/acp-9-5785-2009